

Anisotropic-ray-theory rays in velocity model SC1_II with a split intersection singularity

Luděk Klimeš & Petr Bulant

*Department of Geophysics, Faculty of Mathematics and Physics, Charles University in Prague, Ke Karlovu 3, 121 16 Praha 2, Czech Republic,
<http://sw3d.cz/staff/klimes.htm>, <http://sw3d.cz/staff/bulant.htm>*

Summary

We show the behaviour of the anisotropic-ray-theory S-wave rays in a velocity model with a split intersection singularity. The rays crossing the split intersection singularity are smoothly but very sharply bent. We demonstrate the abrupt changes of geometrical spreading and wavefront curvature of the faster anisotropic-ray-theory S wave. We also demonstrate the formation of caustics and wavefront triplication of the slower anisotropic-ray-theory S wave.

Keywords

Wave propagation, elastic anisotropy, heterogeneous media, anisotropic ray theory, ray tracing, S-wave singularities.

1. Introduction

In a generally anisotropic medium, the S-wave slowness sheets of the slowness surface are usually mostly separated and intersect in at up to 32 point S-wave singularities (Vavryčuk, 2005a; 2005b). In this case, outside the point singularities, the anisotropic-ray-theory rays stay at the faster or slower S-wave slowness sheet, respectively. When approaching the point singularities, the limiting case again corresponds to staying at the faster or slower S-wave slowness sheet, respectively. In a generally anisotropic medium, we thus have to separate the slowness surface into the P-wave slowness sheet, the faster S-wave slowness sheet and the slower S-wave slowness sheet.

However, in a transversely isotropic medium, the S-wave slowness sheets may intersect along intersection singularities (Vavryčuk, 2003). In this special case, we can separate the slowness surface into the P-wave slowness sheet, the SH-wave slowness sheet and the SV-wave slowness sheet, and trace the SH and SV rays. We must know a priori whether the medium is transversely isotropic. We cannot determine it numerically because any rounding error can perturb a transversely isotropic medium to a generally anisotropic medium and split the unstable intersection singularity (Crampin, 1981).

If a medium is close to transversely isotropic but is not transversely isotropic, the intersection singularity is split, the slower S-wave slowness sheet separates from the faster S-wave slowness sheet, forming smooth but very sharp edges on both sheets.

When the slowness vector of a ray smoothly passes through a split intersection singularity or close to the vicinity of a conical or wedge singularity, the ray-velocity vector rapidly changes its direction and creates a sharp bend of the ray. This sharp bend is connected with a rapid rotation of the eigenvectors of the Christoffel matrix.

The sharply bent rays thus cannot describe the correct wave propagation and indicate a failure of the anisotropic ray theory.

While physically reasonable anisotropic-ray-theory rays represent better reference rays for calculating the corresponding arrivals of the prevailing frequency approximation of the coupling ray theory (Klimeš & Bulant, 2012) than the common anisotropic S-wave rays, the sharply bent rays are worse reference rays than the common anisotropic S-wave rays.

The sharply bent rays can safely be traced by solving Hamilton's equations of rays, but we cannot solve the equations of geodesic deviation (paraxial ray equations, dynamic ray tracing equations) numerically along these rays.

In this paper, we shall show the examples of the sharply bent anisotropic-ray-theory rays in velocity model SC1_II which contains a split intersection singularity.

Pšenčík, Farra & Tessmer (2012) used velocity model SC1_II to compare synthetic seismograms calculated by different ray theories with the seismograms calculated by Fourier pseudospectral method. They obtained considerable differences between the seismograms for shallow receivers and concluded that the coupling ray theory along common anisotropic S-wave rays failed because the slowness vectors corresponding to the two anisotropic-ray-theory rays have too different orientation and it is impossible to approximate them by the slowness vector of the common anisotropic S-wave ray. Bulant, Pšenčík, Farra & Tessmer (2011) and Klimeš & Bulant (2012) calculated the same coupling-ray-theory synthetic seismograms using the package CRT and obtained similar errors in the seismograms in the shallow receivers.

In order to check the above mentioned hypothesis, we tried to trace the anisotropic-ray-theory rays in the model SC1_II. Because the phase-velocity section shown by Pšenčík, Farra & Tessmer (2011, fig 11) indicated possible existence of the intersection singularity above the original surface of the model, we decided to extend the model in the vertical direction, and we added 13 new receivers above the original vertical receiver profile.

2. Velocity model SC1_II

At the depth of 0 km, velocity model SC1_II is transversely isotropic with the tilted axis of symmetry. At this depth, the slowness surface contains an intersection singularity. At the depth of 1.5 km, velocity model SC1_II is very close to isotropic, but is slightly cubic and its symmetry axes coincide with the coordinate axes. This means that, at all depths except 0 km, velocity model SC1_II is very close to transversely isotropic, but is slightly tetragonal. Whereas the transversely isotropic medium contains the intersection singularity through which the rays pass without rotation of the eigenvectors of the Christoffel matrix (Vavryčuk, 2001, sec. 4.3), in the slightly tetragonal medium, the S-wave slowness surface is split at this unstable singularity (Crampin, 1981) and the eigenvectors of the Christoffel matrix rapidly rotate by 90° there.

3. Initial-value tracing of anisotropic-ray-theory S-wave rays

Previous versions of the SW3D software package CRT were designed to trace the anisotropic-ray-theory P-wave rays and the common anisotropic S-wave rays using the average S-wave Hamiltonian function according to Klimeš (2006). We did not consider anisotropic-ray-theory S-wave rays for obvious problems with S-wave slowness surface singularities. Now we have added an optional possibility to calculate anisotropic-ray-theory S-wave rays to the package CRT version 7.10 (Bucha & Bulant, 2014) for testing purposes.

Optional tracing of anisotropic-ray-theory S-wave rays is designed for general anisotropy with point S-wave singularities only. We thus a priori choose the faster S wave or the slower S wave. In each step of anisotropic-ray-theory S-wave ray tracing, the Christoffel matrix is calculated together with its eigenvalues and corresponding eigenvectors. We then select the a priori chosen anisotropic-ray-theory S wave (the slower one or the faster one) for the calculation of the ray.

The rays of the selected anisotropic-ray-theory S wave can safely be traced by solving Hamilton's equations of rays. Unfortunately, the equations of geodesic deviation (paraxial ray equations, dynamic ray tracing equations) contain the second-order derivatives of the Hamiltonian function with respect to the slowness vector. Expressions for these derivatives contain the difference of the S-wave eigenvalues of the Christoffel matrix in the denominator. If the difference of the S-wave eigenvalues of the Christoffel matrix is smaller than the rounding error, the second-order derivatives of the Hamiltonian function with respect to the slowness vector become random and, in consequence, the matrix of geometrical spreading becomes random, too. If we wish the rays with a reasonably defined matrix of geometrical spreading and a reasonably defined phase shift due to caustics, we have to terminate tracing of a ray if the relative difference between the S-wave eigenvalues of the Christoffel matrix is smaller than the prescribed limit which we named `DSWAVE`. The maximum angular numerical error of the eigenvectors of the Christoffel matrix in radians is then roughly equal to the ratio of the relative rounding error to parameter `DSWAVE`.

4. Rays in velocity model SC1_II

We calculated rays approximately leading to the receivers located in a vertical well at a distance of 1 km from the source. The receivers extend from the depth of 1.32 km below the source to the elevation of 0.48 km above the source with spacing of 0.04 km. Klimeš & Bulant (2012) considered the 33 receivers below the source only. In this paper, we added the receiver at the source level and the 12 receivers above the source in order to demonstrate the sharp bends of rays and wavefront triplication.

In order to overcome the problems with tracing the S-wave anisotropic-ray-theory rays described by Bulant & Klimeš (2014), we chose `DSWAVE=0.000 000 000 01` and removed the `KMAH` index from ray histories. We then traced the faster S-wave anisotropic-ray-theory rays, the slower S-wave anisotropic-ray-theory rays, and common anisotropic S-wave rays.

The faster S-wave anisotropic-ray-theory rays are displayed in Figures 1 and 2. Due to the constant vertical gradient of elastic moduli, the slowness vectors slowly rotate during ray tracing. The slowness vectors of the rays leading to the receivers from the second receiver below the source to the ninth receiver above the source cross the split

intersection singularity. Crossing the split intersection singularity results in smooth but very sharp bends of rays. These sharp bends are connected with a rapid rotation of the eigenvectors of the Christoffel matrix. The sharply bent rays thus cannot describe the correct wave propagation and indicate a failure of the anisotropic ray theory. The related abrupt change of the anisotropic-ray-theory amplitude between the second and third receivers below the source (and also between the ninth and tenth receivers above the source) also suggests that the anisotropic ray theory is not applicable there.

The slower S-wave anisotropic-ray-theory rays are displayed in Figures 3 and 4. The sharply bent slower S-wave anisotropic-ray-theory rays lead to the receivers from the first receiver above the source to the third receiver above the source. These rays are bent in the opposite direction than the faster S-wave anisotropic-ray-theory rays, and form the wavefront triplication. The caustics limiting the triplication are positioned between the zeroth and first receivers above the source, and between the third and fourth receivers above the source, respectively.

The common anisotropic S-wave rays, traced using the average S-wave Hamiltonian function according to Klimeš (2006) are displayed in Figure 5. The corresponding geometrical spreading and the corresponding amplitude are very smooth.

The anisotropic-ray-theory rays of the faster S wave, the anisotropic-ray-theory rays of the slower S wave, and the common anisotropic S-wave rays are compared in Figure 6. Although the domain of ray parameters parametrizing the initial slowness vectors of rays is the same for all three kinds of rays, the uppermost anisotropic-ray-theory ray of the slower S wave leads to the seventh receiver above the source, the uppermost common anisotropic S-wave ray leads to the ninth receiver above the source, whereas the anisotropic-ray-theory rays of the faster S wave lead to all receivers including the topmost twelfth receiver above the source.

In Figure 6, we can see that for the receivers located deeper in the model, the common anisotropic S-wave ray is always between the two anisotropic rays and the differences between the rays are not so large. For the shallower receivers starting from the third receiver below the surface of the model, the slower S wave interacts with the singularity and the rays are sharply bent at the singularity. As the result of this bending, the common anisotropic rays are no more situated between the two anisotropic rays. Starting from the first receiver above the source, also the faster S wave is bent by the singularity, which results in even higher difference between the trajectories of the common anisotropic S-wave ray and of the anisotropic-ray-theory S-wave rays. At the faster S wave, the singularity generates a triplication.

5. Ray parameters of traced rays

The two-point rays leading to the receivers have been searched for using the algorithm by Bulant (1996; 1999), with the KMAH index removed from ray histories.

Ray parameters of the anisotropic-ray-theory rays of the faster S wave are displayed in Figures 7 and 8. The ray parameters of the two-point rays approximately leading to the receivers (large red crosses) can be divided into three segments. The left-hand segment corresponds to three smooth rays leading to the twelfth, eleventh and tenth receivers above the source in Figure 1. The middle segment corresponds to 12 sharply bent rays leading to the receivers from the ninth receiver above the source to the second receiver below the source in Figure 1. The paraxial approximation used in the algorithm by Bulant (1996; 1999) to find the two-point rays inevitably failed in this middle segment, which is obvious from the distribution of auxiliary rays shot towards the receivers. The right-hand segment corresponds to 31 smooth rays leading to the receivers from the third receiver below the source to the 33rd receiver below the source in Figure 1.

Ray parameters of the anisotropic-ray-theory rays of the slower S wave are displayed in Figures 9 and 10. The ray parameters of the two-point rays approximately leading to the receivers (large red crosses) can be divided into three segments. The left-hand segment corresponds to seven smooth rays leading to the receivers from the seventh receiver above the source to the first receiver above the source in Figure 3. The middle segment corresponds to 3 sharply bent rays leading to the first, second and third receivers above the source in Figure 3. Since the KMAH index has been disabled, the caustics do not affect the ray history of these rays. The paraxial approximation used in the algorithm by Bulant (1996; 1999) to find the two-point rays inevitably failed in this middle segment, which is obvious from the distribution of auxiliary rays shot towards the receivers. The right-hand segment corresponds to 37 smooth rays leading to the receivers from the third receiver above the source to the 33rd receiver below the source in Figure 3.

There is no problem with two-point tracing the common anisotropic S-wave rays, see Figure 11.

6. Conclusions

In velocity models with split intersection singularity at the slowness surface, the S-wave anisotropic-ray-theory rays do not describe the actual paths of wave propagation and do not represent reasonable reference rays for the coupling ray theory. In this case, the common anisotropic S-wave rays represent much better reference rays for the coupling ray theory.

If the common anisotropic S-wave rays are not sufficiently close to the actual paths of wave propagation or the corresponding common S-wave amplitudes are not sufficiently accurate for both S-wave arrivals, we may consider approximate SH and SV reference rays. To trace the approximate SH and SV reference rays, we approximate the correct velocity model by a transversely isotropic velocity model and trace these rays. We then apply the prevailing-frequency approximation of the coupling ray theory along the SH and SV reference rays (Klimeš & Bulant, 2014) to the correct velocity model.

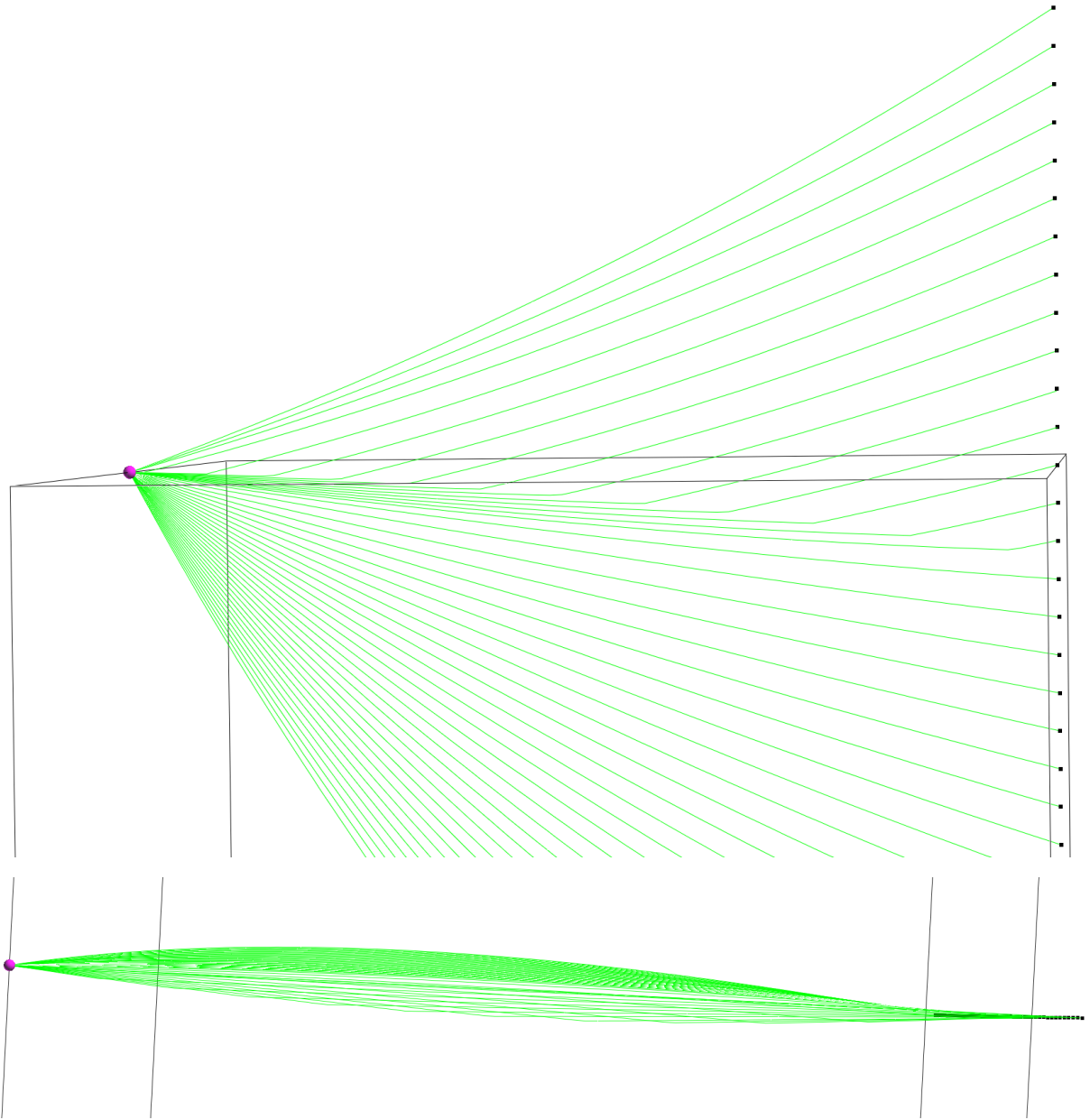


Figure 1: Front view and top view of the anisotropic-ray-theory rays of the faster S wave. It is obvious how the geometrical spreading increases behind the sharp bends of rays.

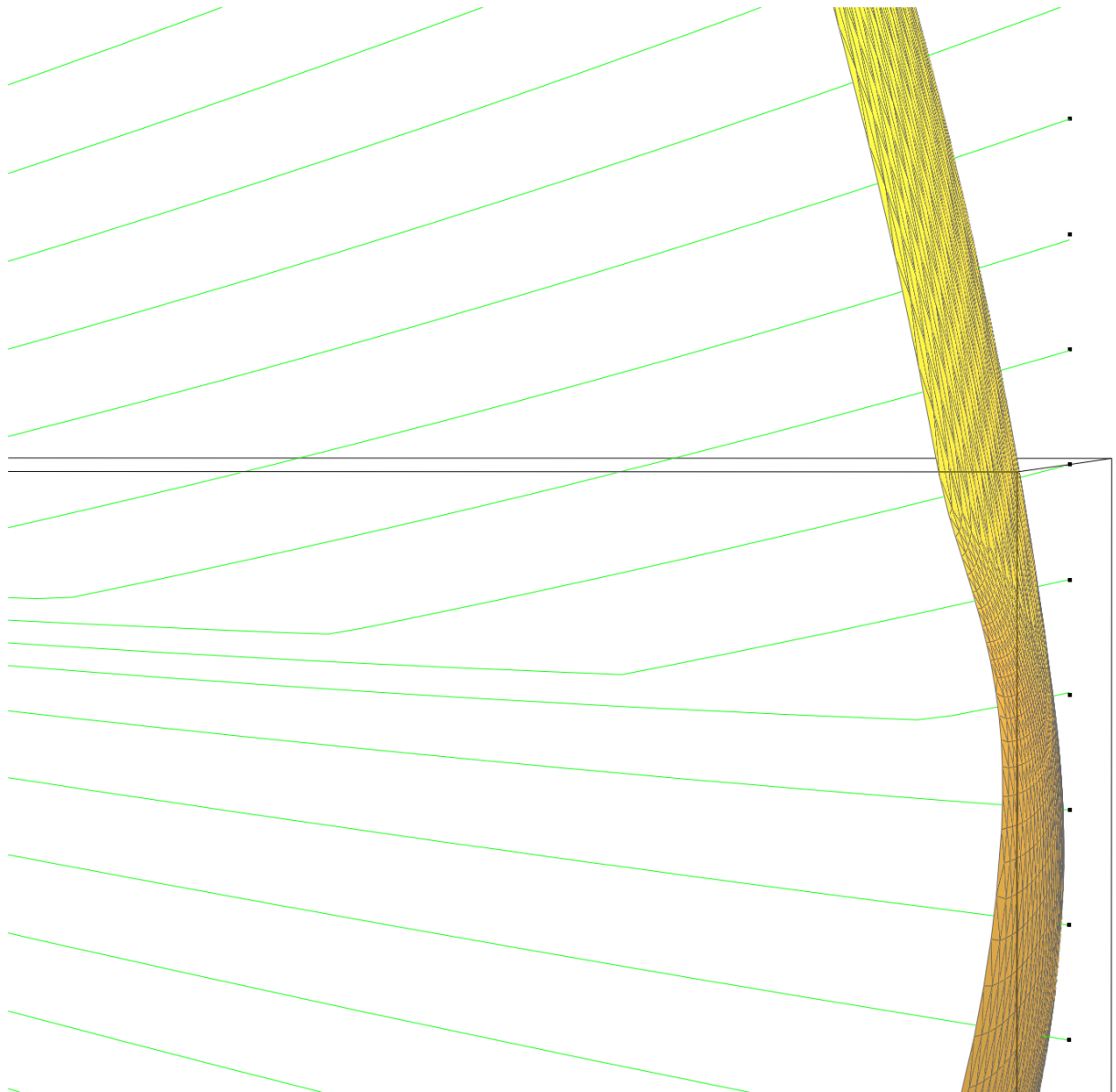


Figure 2: Detail of the anisotropic-ray-theory rays of the faster S wave together with a wavefront. We can clearly observe considerable decrease of the wavefront curvature behind the sharp bends of rays.

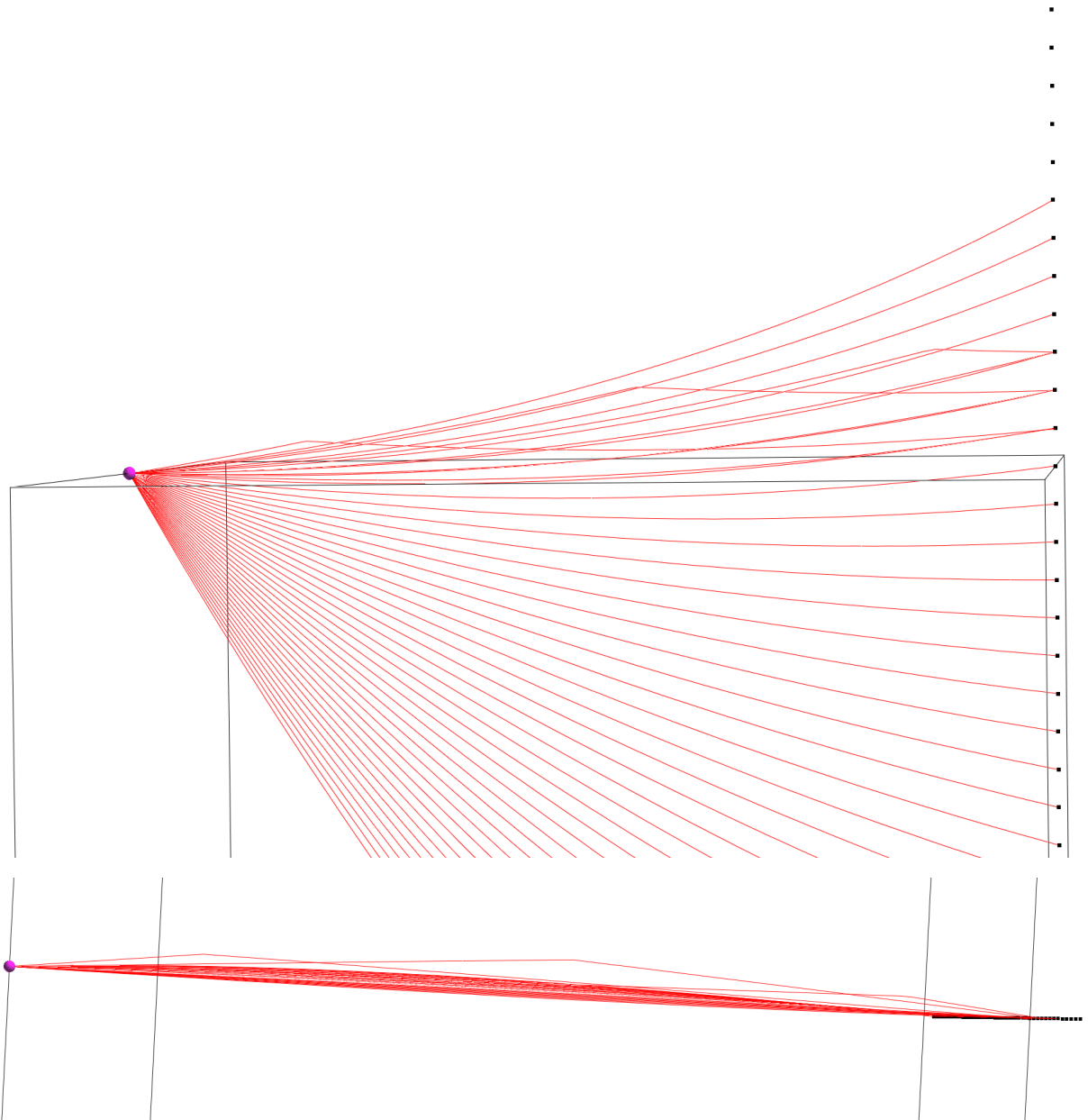


Figure 3: Front view and top view of the anisotropic-ray-theory rays of the slower S wave. We can clearly observe the caustics caused by the sharply bent rays and the formation of the wavefront triplication at the first, second and third receivers above the source.

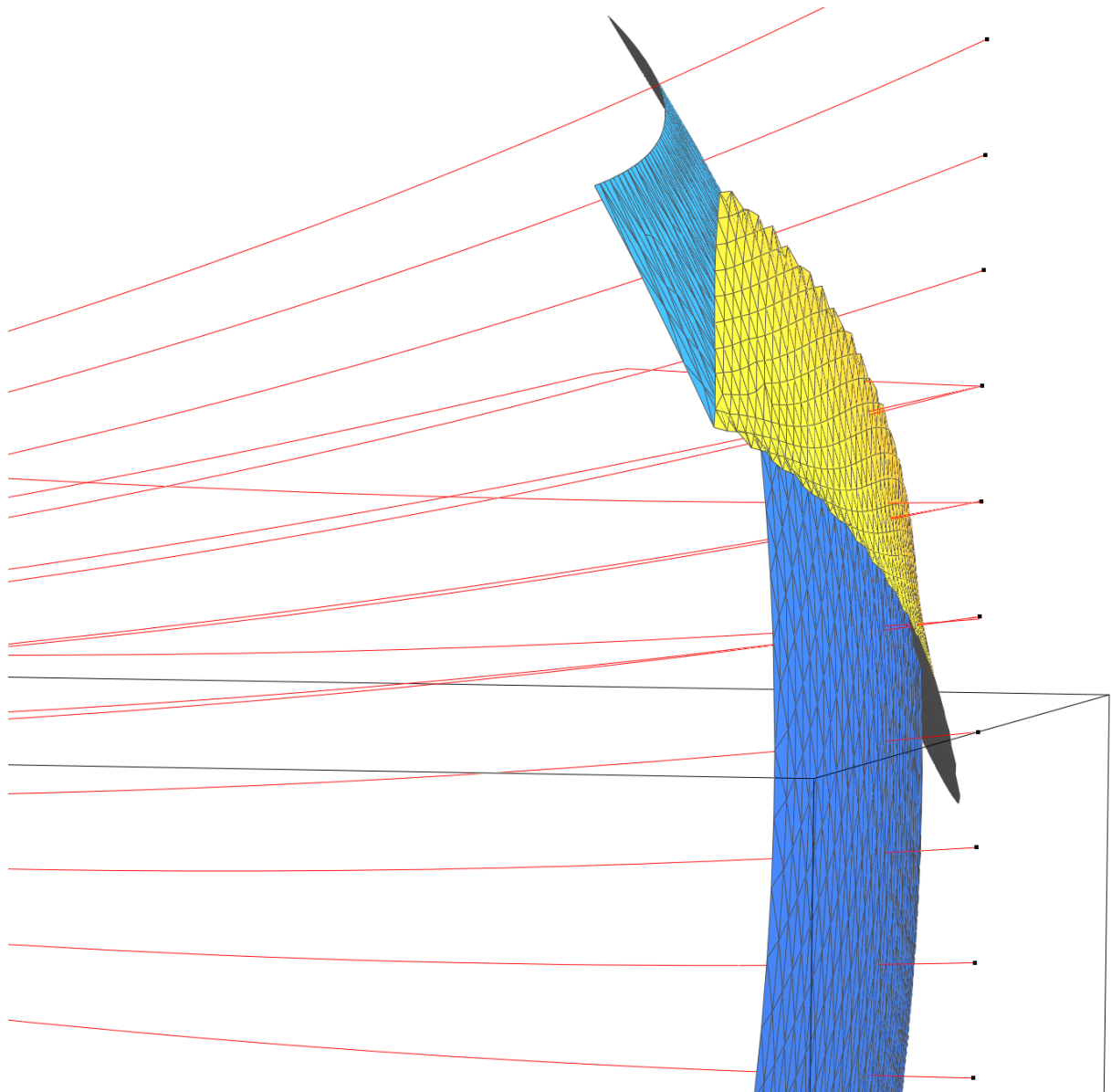


Figure 4: Detail of the anisotropic-ray-theory rays of the slower S wave together with a wavefront containing the triplication.

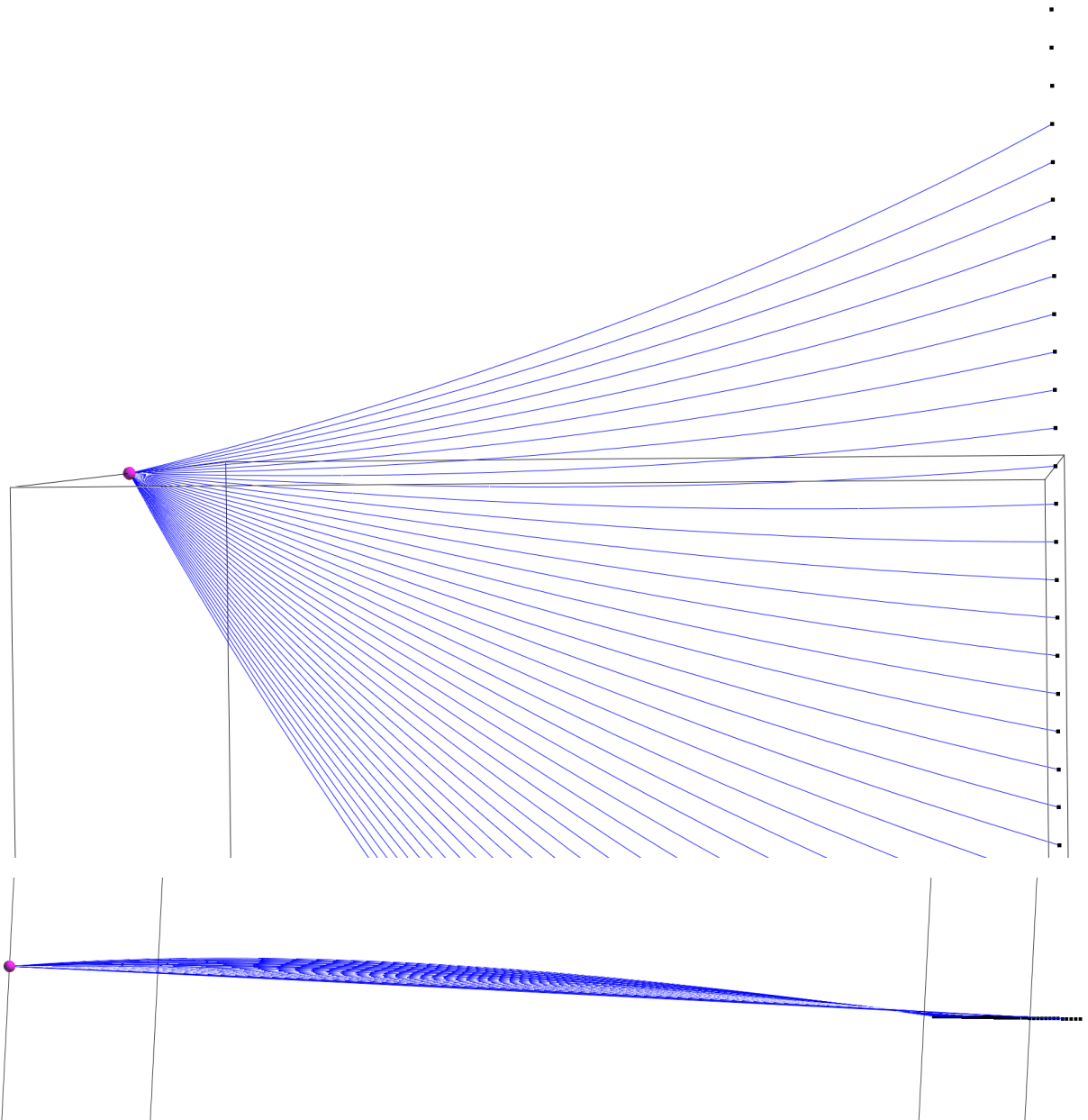


Figure 5: Front view and top view of the common anisotropic S-wave rays. The corresponding geometrical spreading and the corresponding amplitude are very smooth.

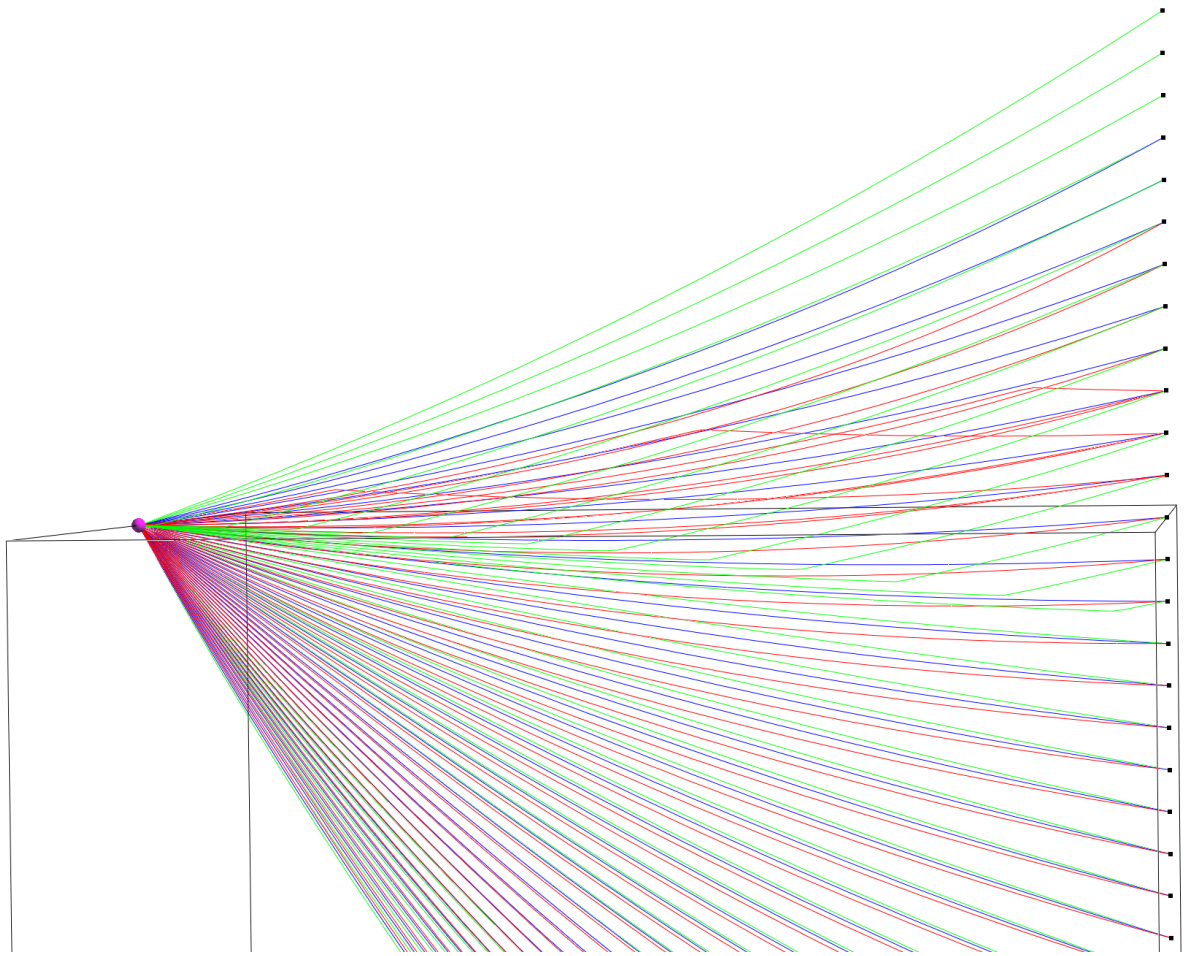


Figure 6: Common front view of the anisotropic-ray-theory rays of the faster S wave (green), anisotropic-ray-theory rays of the slower S wave (red), and anisotropic common S-wave rays (blue).

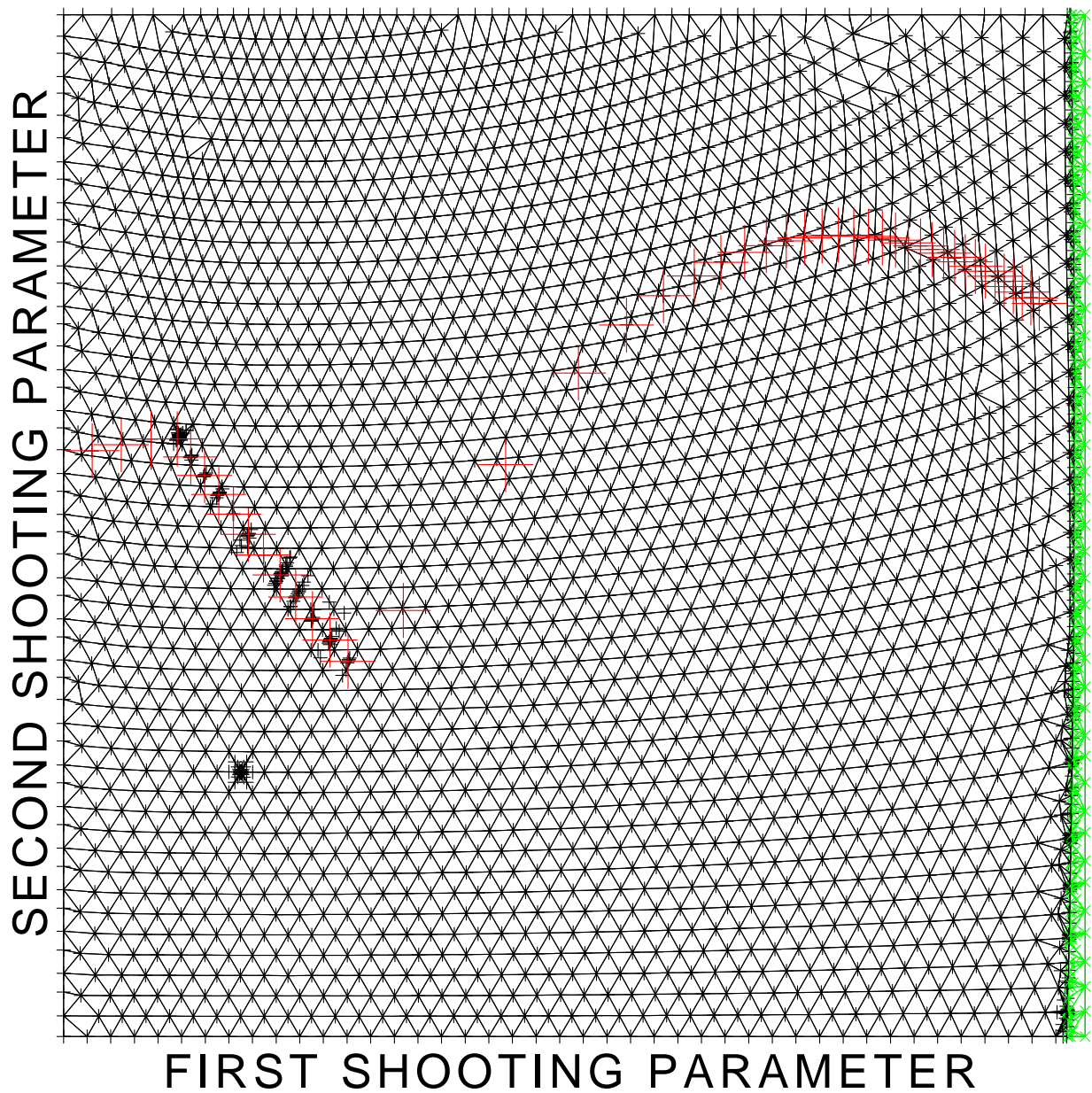


Figure 7: Ray parameters of all traced anisotropic-ray-theory rays of the faster S wave, including the triangulation of the ray-parameter domain. The large red crosses correspond to the rays approximately leading to the receivers. It is obvious from the distribution of auxiliary rays shot towards the receivers that the paraxial approximation inevitably failed in the belt of sharply bent rays. The left bottom isolated cluster of auxiliary rays corresponds to the ray which could not be traced, refer to the blue diamond in Figure 8.

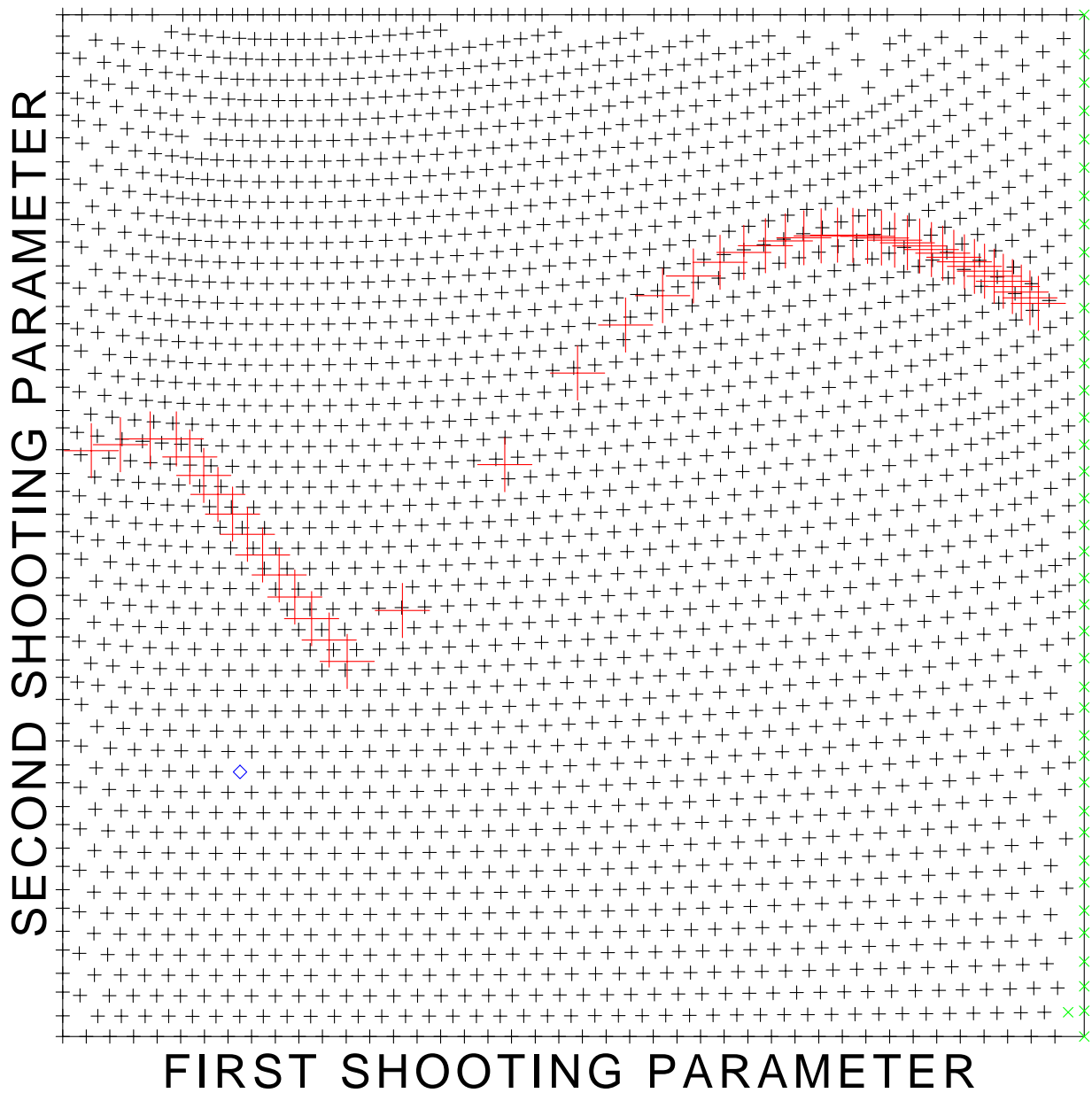


Figure 8: Ray parameters of the basic system of the anisotropic-ray-theory rays of the faster S wave, together with the rays approximately leading to the receivers. The black plus crosses correspond to the rays incident at the receiver side of the velocity model. The large red plus crosses correspond to the rays approximately leading to the receivers. The green times crosses correspond to the rays incident at the bottom of the velocity model. The blue diamond corresponds to the ray whose tracing was terminated, which may be caused by a too close point S-wave singularity somewhere along the ray.

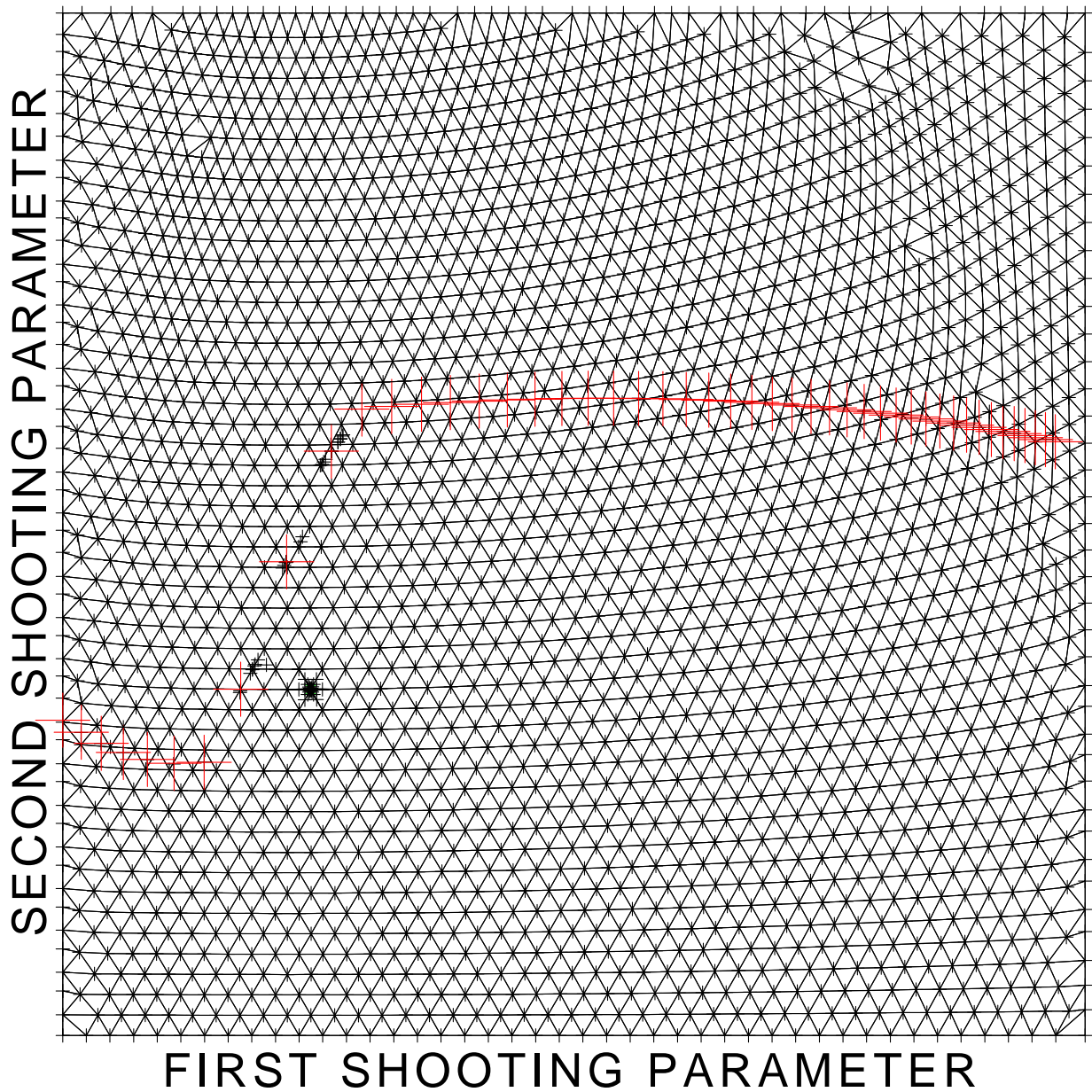


Figure 9: Ray parameters of all traced anisotropic-ray-theory rays of the slower S wave, including the triangulation of the ray-parameter domain. The large red crosses correspond to the rays approximately leading to the receivers. It is obvious from the distribution of auxiliary rays shot towards the receivers that the paraxial approximation inevitably failed in the belt of sharply bent rays. The isolated cluster of auxiliary rays corresponds to the ray which could not be traced, refer to the green times cross in Figure 10.

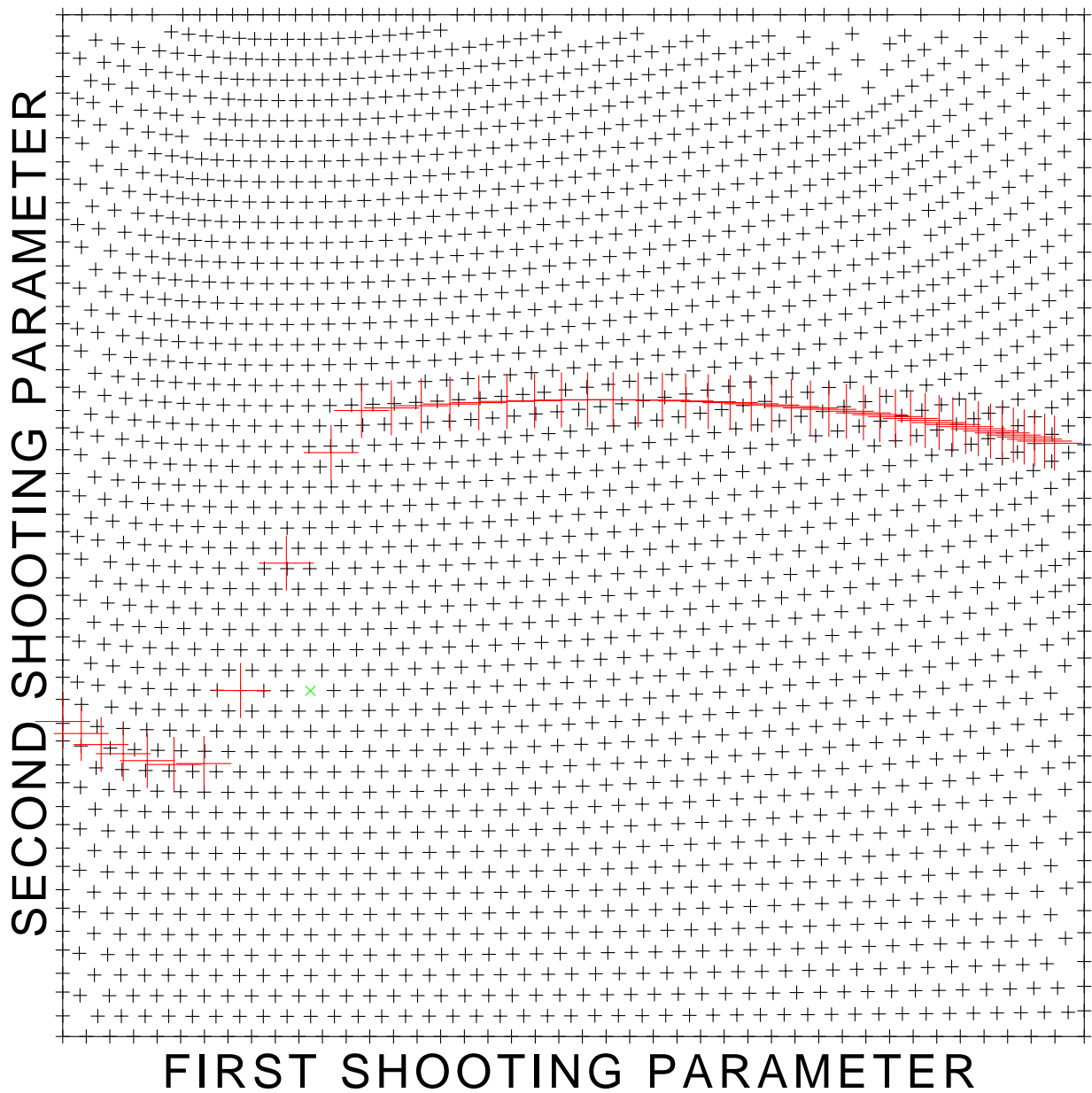


Figure 10: Ray parameters of the basic system of the anisotropic-ray-theory rays of the slower S wave, together with the rays approximately leading to the receivers. The black plus crosses correspond to the rays incident at the receiver side of the velocity model. Since the KMAH index has been disabled, the caustics do not affect the ray history. The large red plus crosses correspond to the rays approximately leading to the receivers. The green times cross corresponds to the ray whose tracing was terminated, which may be caused by a too close point S-wave singularity somewhere along the ray.

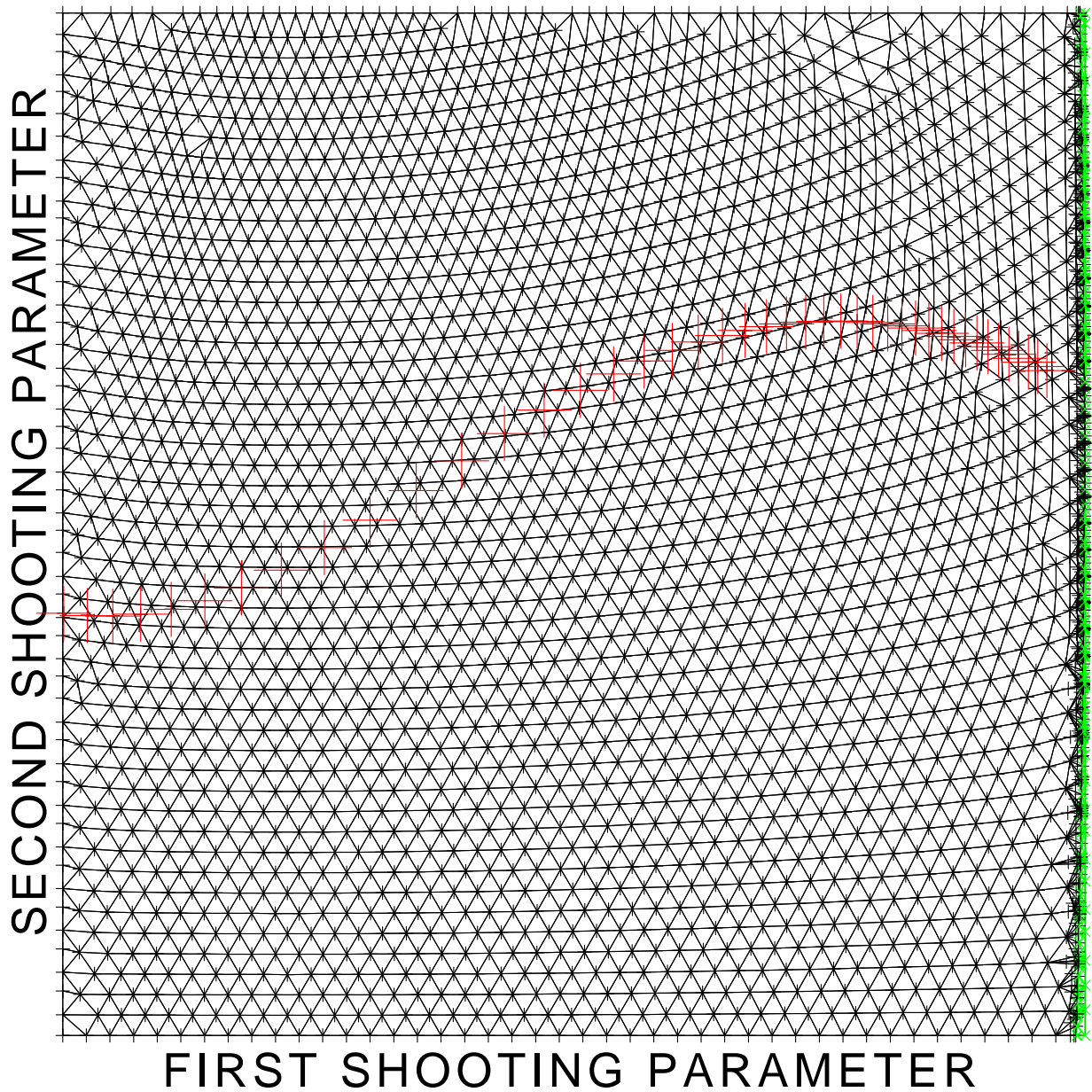


Figure 11: Ray parameters of all traced common anisotropic S-wave rays, including the triangulation of the ray-parameter domain. The black plus crosses correspond to the rays incident at the receiver side of the velocity model. The large red plus crosses correspond to the two-point rays leading to the receivers. The green times crosses correspond to the rays incident at the bottom of the velocity model. The paraxial approximation efficiently determined the two-point rays leading to the receivers, without superfluous auxiliary rays.

Acknowledgements

The research has been supported by the Grant Agency of the Czech Republic under contract P210/10/0736, by the Ministry of Education of the Czech Republic within research projects MSM0021620860 and CzechGeo/EPOS LM2010008, and by the members of the consortium “Seismic Waves in Complex 3-D Structures” (see “<http://sw3d.cz>”).

References

- Bucha, V. & Bulant, P. (eds.) (2014): SW3D-CD-18 (DVD-ROM). *Seismic Waves in Complex 3-D Structures*, **23**, 211–212, online at “<http://sw3d.cz>”.
- Bulant, P. (1996): Two-point ray tracing in 3-D. *Pure appl. Geophys.*, **148**, 421–447.
- Bulant, P. (1999): Two-point ray-tracing and controlled initial-value ray-tracing in 3-D heterogeneous block structures. *J. seism. Explor.*, **8**, 57–75.
- Bulant, P. & Klimeš, L. (2014): Anisotropic-ray-theory geodesic deviation and two-point ray tracing through a split intersection singularity. *Seismic Waves in Complex 3-D Structures*, **24**, 179–187, online at “<http://sw3d.cz>”.
- Bulant, P., Pšenčík, I., Farra, V. & Tessmer, E. (2011): Comparison of the anisotropic-common-ray approximation of the coupling ray theory for S waves with the Fourier pseudo-spectral method in weakly anisotropic models. In: *Seismic Waves in Complex 3-D Structures, Report 21*, pp. 167–183, Dep. Geophys., Charles Univ., Prague, online at “<http://sw3d.cz>”.
- Crampin, S. (1981): A review of wave motion in anisotropic and cracked elastic-media. *Wave Motion*, **3**, 343–391.
- Klimeš, L. (2006): Common-ray tracing and dynamic ray tracing for S waves in a smooth elastic anisotropic medium. *Stud. geophys. geod.*, **50**, 449–461.
- Klimeš, L. & Bulant, P. (2012): Single-frequency approximation of the coupling ray theory. In: *Seismic Waves in Complex 3-D Structures, Report 22*, pp. 143–167, Dep. Geophys., Charles Univ., Prague.
- Klimeš, L. & Bulant, P. (2014): Prevailing-frequency approximation of the coupling ray theory for S waves along the SH and SV reference rays in a transversely isotropic medium. *Seismic Waves in Complex 3-D Structures*, **24**, 165–177, online at “<http://sw3d.cz>”.
- Pšenčík, I., Farra, V. & Tessmer, E. (2012): Comparison of the FORT approximation of the coupling ray theory with the Fourier pseudospectral method. *Stud. geophys. geod.*, **56**, 35–64.
- Vavryčuk, V. (2001): Ray tracing in anisotropic media with singularities. *Geophys. J. int.*, **145**, 265–276.
- Vavryčuk, V. (2003): Generation of triplications in transversely isotropic media. *Phys. Rev. B*, **68**, 054107-1–054107-8.
- Vavryčuk, V. (2005a): Acoustic axes in weak triclinic anisotropy. *Geophys. J. int.*, **163**, 629–638.
- Vavryčuk, V. (2005b): Acoustic axes in triclinic anisotropy. *J. acoust. Soc. Am.*, **118**, 647–653.